Nanoscale

Accepted Manuscript

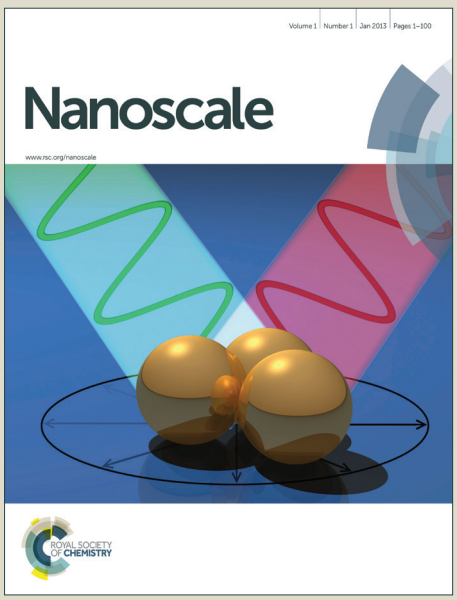

ROYAL SOCIETY OF CHEMISTRY

www.rsc.org/nanoscale

Journal Name

RSCPublishing

ARTICLE

Multifunctional Au-Fe_3O_4@MOF core-shell nanocomposite catalysts with controllable reactivity and magnetic recyclability

Fei Ke[ab], Luhuan Wang[a], and Junfa Zhu*[a]

Cite this: DOI: 10.1039/xoxxoooooox

Received ooth January 2012,
Accepted ooth January 2012

DOI: 10.1039/xoxxoooooox

www.rsc.org/

Recovery and reuse of expensive catalysts are important in both heterogeneous and homogenous catalysis due to economic and environmental reasons. This work reports a novel multifunctional magnetic core-shell gold catalyst which can be easily prepared and shows remarkable catalytic property in the reduction of 4-nitrophenol. The novel Au-Fe_3O_4@metal-organic framework (MOF) catalyst consists of a superparamagnetic Au-Fe_3O_4 core and a porous MOF shell with controllable thickness. Small Au nanoparticles (NPs) of 3-5 nm are mainly sandwiched between the Fe_3O_4 core and porous MOF shell. Catalytic studies show that the core-shell structured Au-Fe_3O_4@MOF catalyst has much higher catalytic activity than other reported Au-based catalysts toward the reduction of 4-nitrophenol. Moreover, this catalyst can be easily recycled due to the presence of the superparamagnetic core. Therefore, compared to conventional catalysts used in the reduction of 4-nitrophenol, this porous MOF-based magnetic catalyst is green, cheap and promising for industrial applications.

Introduction

Functional nanocomposites represent an important class of nanomaterials and have attracted increased research interests due to their superior properties compared with individual components.[1] As an important member of nanocomposites family, magnetic nanocomposites with defined nanostructures have been intensively investigated because of their multi-disciplinary applications, such as magnetic resonance imaging, targeted drug delivery, pollution clean-up, data storage, and catalysis.[2-5] Among a multitude of magnetic nanocomposites investigated, magnetic materials and noble metal-based hybrid nanocrystals, such as Au-Fe_3O_4, Ag-Fe_3O_4, and Pt-Fe_3O_4, have received special attention due to their novel properties and unique applicability which cannot be achieved for single component nanocrystals.[6] Recently, Fe_3O_4@Au core-shell NPs is an even more attractive nanocomposite system, not only due to its high catalytic activity and chemical stability but also because it can be readily functionalized through the well-developed Au-N or Au-S chemistry.[7] However, several unavoidable factors associated with these magnetic nanocomposites, such as the tendency to aggregate in order to reduce the surface energy, and the intrinsic instability under harsh reaction conditions which results in the loss of their initial activity and dispersibility,[8] hinder their applications. Therefore, great efforts have been devoted to develop novel strategies to stabilize NPs. So far, the most common approach is to coat noble-metal NPs with mesoporous silica shells. The mesoporous silica shells not only endow NPs with high stability but also offer them additional functionalities.[9,10] However, these magnetic mesoporous materials suffer from long synthetic steps, sacrificial templates, and high reaction temperature, which make them too expensive for widespread industrial use.

MOFs (also known as porous coordination polymers) are a burgeoning class of crystalline materials comprising inorganic nodes and organic linkers.[11] These materials have unquestionably enormous potential for many practical applications, such as selective gas adsorption and separation,[12] sensing,[13] drug delivery.[14-17] and catalysis.[18,19] MOFs have uniform but tunable cavities, tailorable chemistry and are suited to stabilize small metal NPs without blocking their surfaces, making them very attractive in catalysis. To date, several technologies such as solution infiltration,[20] solid grinding,[21] surface grafting[22] and metal-organic chemical vapor deposition (MOCVD)[23] have been developed for incorporating metal NPs into MOFs. Unfortunately, in these post-synthesis incorporation methods, the porous structure of the MOF was sometimes damaged, and the agglomeration of NPs was commonly observed.[24] A preferred strategy, coating the MOF on the preformed NPs, was recently reported.[25] Using this strategy, we have reported a novel porous Au@MIL-100(Fe) core-shell catalyst with a controlled MIL-100(Fe) shell thickness, which exhibits high catalytic performance in the reduction of 4-nitrophenol (4-NP) to 4-aminophenol (4-AP) in water.[26] However, although this catalyst is recyclable, it is not easy.

Herein, we report a highly active and easily recycled MOF-based porous magnetic core-shell Au catalyst, i.e., Au-Fe_3O_4@MIL-100(Fe). The catalyst was synthesized by a versatile layer-by-layer assembly method. The shell thickness in core-shell structures can be controlled by adjusting the assembly cycle number. To improve the recyclability, we incorporate a superparamagnetic Fe_3O_4 core at the center of the initial catalysts (Fig. 1). Although several steps are required, the overall synthesis is highly reproducible. The designed porous magnetic catalysts show excellent dual functions which can not only undergo rapid catalytic reduction of 4-NP to 4-AP but also can be easily recycled using an external magnetic field. To our best knowledge, this is the first report demonstrating the use of Au-Fe_3O_4@MIL-100(Fe) core-shell structures as magnetically recyclable catalyst for efficient reduction of nitroaromatic compound.

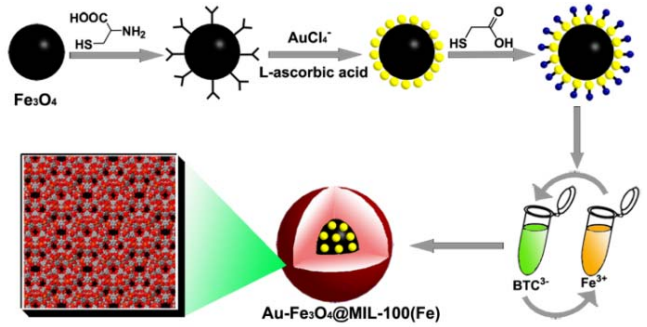

Fig. 1 Schematic representation of the preparation of the Au-Fe_3O_4@MIL-100(Fe) core-shell magnetic NPs by a layer-by-layer strategy. The Au NPs were first immobilized on the surface of the L-cysteine-modified Fe_3O_4 NPs by using L-ascorbic acid as the reductive agent, followed by functionalizing with mercaptoacetic acid (MAA). Then, the Au-Fe_3O_4@MIL-100(Fe) core-shell catalyst was prepared by repeated cycles of dispersing the MAA-functionalized Au-Fe_3O_4 NPs into the ethanol solution of $FeCl_3$ and H_3BTC separately at 70 °C. The overall shell thickness can be controlled by adjusting the assembly cycle number.

Experimental Section

Materials

Benzene-1,3,5-tricarboxylic acid (H_3BTC) was purchased from Aldrich. Tetrachloroauric acid tetrahydrate, ferric trichloride hexahydrate, sodium acetate trihydrate, L-cysteine, L-ascorbic acid, ethylene glycol, and thioglycollic acid were purchased from Sinopharm (Shanghai) Chemical Reagent Co., Ltd., China. All other chemicals used in this work were of analytical grade, obtained from commercial suppliers, and used without further purification unless otherwise noted.

Characterization

The powder X-ray diffraction (PXRD) pattern of the sample was collected using an X-ray diffractometer with Cu target (36 kV, 25 mA) from 2 to 70°. The morphology of the samples was monitored with a FEI Tecnai G2 F20 transmission electron microscope at 200 keV. Nitrogen adsorption-desorption isotherm was obtained at 77 K on a Micromeritics TriStar II 3020 adsorption analyzer. The magnetization curve was measured at room temperature under a varying magnetic field from -20000 to 20000 Oe on a BHV-55 vibrationg sample magnetometer (VSM). The UV-vis absorption spectra were recorded on a Shimadzu UV-1800 spectrophotometer. The X-ray absorption spectroscopy (XAS) measurements were performed at the 4W1B beamline in Beijing Synchrotron Radiation Facility (BSRF).

Synthesis of Au-Fe_3O_4 NPs.

Fe_3O_4 NPs were synthesized by a solvothermal reaction as reported previously.[27] (a) For L-cysteine-functionalized Fe_3O_4 NPs, 20 mg Fe_3O_4 NPs were pretreated with HCl aqueous solution (5 mL, 1 M) under ultrasound for 5 min. Then the magnetic NPs were recovered by a permanent magnet and thoroughly washed several times with distilled water and redispersed in mixture of distilled water (20 mL) and L-cysteine aqueous solution (10 mL, 10 g L^{-1}) with ultrasonication for 1 h. Subsequently, the product was separated by the permanent magnetic and washed with distilled water, and redispersed in distilled water (20 mL). (b) For the synthesis of Au-Fe_3O_4 NPs, 2 mL of chloroauric acid (25 mM) was added dropwise into the obtained L-cysteine-functionalized Fe_3O_4 suspension and the mixture solution was stirred for 3 h, followed by addition of 5 mL of L-ascorbic acid (1 wt %) and the mixed solution was stirring for another 3 h. Finally, by the use of the permanent magnet, the product was separated and washed with distilled water and ethanol several times, and then redispersed in ethanol.

Synthesis of mercaptoacetic acid (MAA)-functionalized Au-Fe_3O_4 NPs

MAA-functionalized Au-Fe_3O_4 NPs were prepared according to the following process. The as-synthesized Au-Fe_3O_4 NPs were added to 10 mL of ethanol solution of thioglycollic acid (0.29 mM) under shaking for 24 h. The product was recovered by a permanent magnet and washed several times with ethanol, and then redispersed in ethanol.

Synthesis of core-shell magnetic Au-Fe_3O_4@MIL-100(Fe) NPs

Briefly, 20 mg of MAA-functionalized Au-Fe_3O_4 was immersed in 4 mL of $FeCl_3$ ethanol solution (10 mM) for 15 min and then in 4 mL of H_3BTC ethanol solution (10 mM) for 30 min at 70 °C. Between each step the magnetic NPs were washed with ethanol. After a given number of cycles, the sample was recovered by a permanent magnet and washed with ethanol, and dried under vacuum at 120 °C.

Details for catalytic reaction of reduction of 4-NP to 4-AP

The catalytic reduction of 4-NP by $NaBH_4$ was chosen as a model reaction for testing and comparing the efficiency of the catalysts with different assembly cycles of MOF shell. After stirring a mixture of 162.3 mg of $NaBH_4$ dissolved in 11.3 mL distilled water and 15 mL of 0.18 mM 4-NP for 20 min, 3.4 mg of catalyst (Au-Fe_3O_4 or MIL-100(Fe) or Au-Fe_3O_4@MIL-100(Fe) with different assembly cycles of MOF shell) was added. The bright yellow solution gradually faded as the reaction proceeded, and the UV-vis spectra were recorded at short intervals to monitor the progress of the reaction. The kinetic rate constants of the

reduction process were determined through measuring the change in absorbance at 400 nm as a function of time.

Results and discussion

The crystal structure and porosity of the as-synthesized sample were studied by PXRD and nitrogen adsorption-desorption isotherm. As shown in Figure 2, the PXRD pattern clearly confirms that the product is composed of three components: pure cubic-phase Au (JCPDS file 04-0784),[7] crystalline Fe_3O_4 (JCPDS file 19-0629),[28] and crystalline MIL-100(Fe).[29] No peaks assigned to impurities are observed. The features of the MOF shells, especially the porosity, determine the properties of the core-shell magnetic NPs.[30] Fig. 3 presents the corresponding nitrogen adsorption-desorption isotherm of the sample with a mode intermediate between type I, which is related to microporous materials, and type IV, which is related to mesoporous materials. The presence of a pronounced hysteresis loop in the nitrogen adsorption-desorption isotherm is indicative of a porous structure with a 3D intersection network.[31] The Brunauer-Emmett-Teller (BET) surface area and pore volume of the sample were calculated to be 335.05 $m^2 g^{-1}$ and 0.22 $cm^3 g^{-1}$, respectively. Furthermore, estimation of the pore size distribution by the density functional theory (DFT) shows two pore sizes at 1.59 and 2.16 nm for Au-Fe_3O_4@MIL-100(Fe) core-shell magnetic NPs (Fig. 3, inset), attributed to micropore and mesopore cages, respectively, which is consistent with the previously reported results for MIL-100(Fe) crystals.[32]

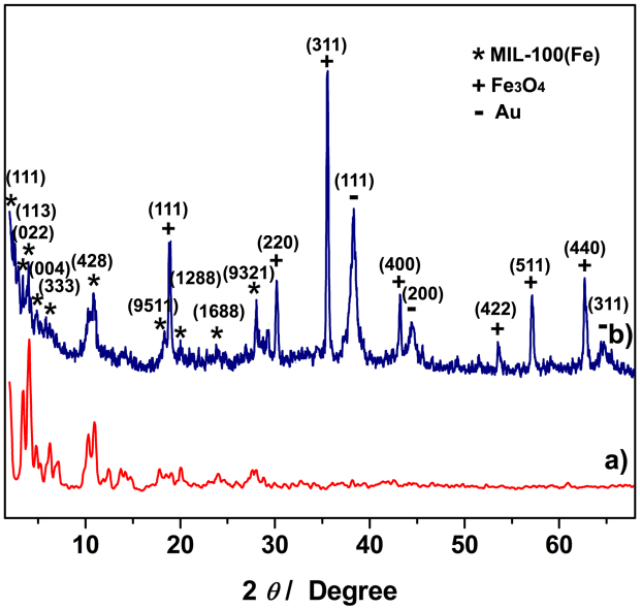

Fig. 2 PXRD patterns of (a) simulated from the crystallographic data of MIL-100(Fe) and (b) Au-Fe_3O_4@MIL-100(Fe) core-shell NPs after 30 assembly cycles.

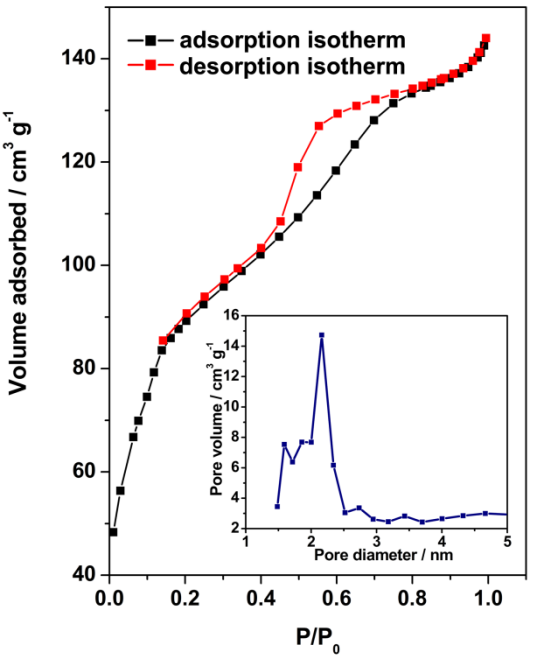

Fig. 3 Nitrogen adsorption-desorption isotherm of the Au-Fe_3O_4@MIL-100(Fe) core-shell magnetic NPs measured at 77 K. The inset shows corresponding pore size distribution analysis obtained using DFT.

Fig. 4 shows the TEM images of Au-Fe_3O_4 and Au-Fe_3O_4@MIL-100(Fe) core-shell magnetic NPs with different assembly cycles. It can be seen that small Au particles uniformly disperse on the surface of Fe_3O_4 particles (Fig. 4a-f). The representative high-resolution TEM (HRTEM) images of Au-Fe_3O_4@MIL-100(Fe) reveal that the size of the Au particles is 3-5 nm (Fig. 4g and h). After these particles assembling with MIL-100(Fe), on the outside surface of the Au-Fe_3O_4 particles (dark part), it forms a porous MOF shell (light part). With increasing the number of the assembly cycles, the thickness of the MOF shell increases (see also Fig. S1 in the Electronic Supplementary Information†). Further statistics based on the products shown in Fig. S1f indicates that both the sizes of the core-shell Au-Fe_3O_4@MIL-100(Fe) magnetic NPs and the shell thickness show nearly linear dependence on the number of assembly cycles. The chemical composition of the core-shell NPs is evidenced by energy dispersive X-ray (EDX) spectroscopy. As can be seen from Fig. S2a, the Au-Fe_3O_4 sample is composed of C, N, O, S, Fe and Au. Moreover, with increasing the number of assembly cycles of MIL-100(Fe) shell, the relative content of Au in the Au-Fe_3O_4@MIL-100(Fe) core-shell magnetic NPs decreases gradually, while the contents of the elements C, O and Fe of MIL-100(Fe) increase, suggesting that the Au NPs core are surrounded with uniform MIL-100(Fe) shell. Moreover, the composition of the core-shell magnetic NPs is obvious in the high-angle annular dark-field scanning TEM (HAADF-STEM) image (Fig. 4i and j), in which Au NPs as the core appears as brighter contrast due to larger atomic mass. The corresponding elemental mapping further indicates that the Au element is homogeneously located only in the core, while the elements C, Fe, and O of MIL-100(Fe) are homogenously distributed

throughout the whole NPs, suggesting that an Au core is surrounded with a uniform MIL-100(Fe) shell. This porous MIL-100(Fe) shell helps the sandwiched small Au NPs to remain stable against coagulation, but at the same time they are still accessible to the reacting species as a catalyst.

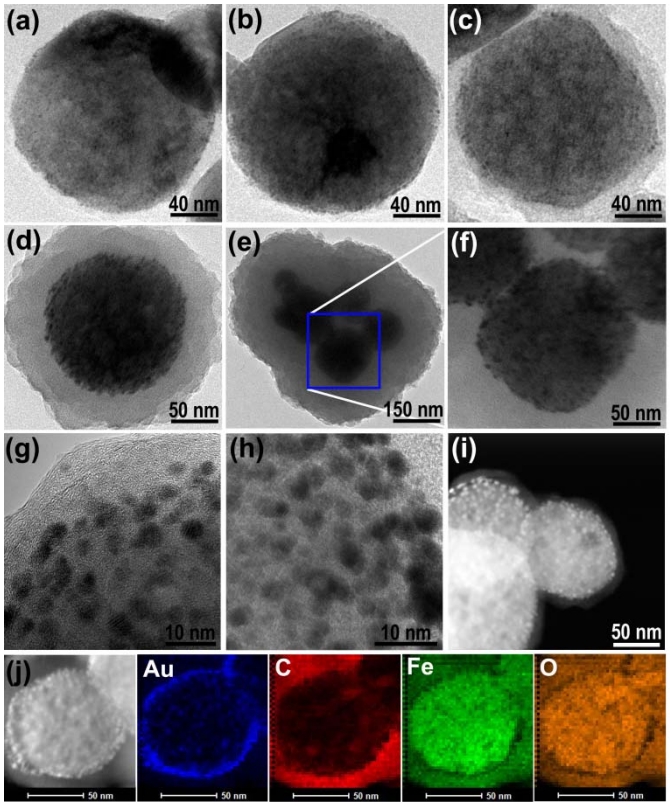

Fig. 4 TEM images of Au-Fe_3O_4 (a) and individual Au-Fe_3O_4@MIL-100(Fe) core-shell magnetic NPs after 5 (b),10 (c), 20 (d), 30 (e and f) assembly cycles. HRTEM and HAADF-STEM images of Au-Fe_3O_4@MIL-100(Fe) core-shell magnetic NPs after 10 (g, i) and 20 (h, j) assembly cycles and the corresponding elemental mappings for Au, C, Fe and O elements.

The magnetic property of the as-synthesized Au-Fe_3O_4@MIL-100(Fe) core-shell magnetic NPs was investigated at 300 K using VSM in the field range from -20 to +20 KOe. The saturated magnetization value of the core-shell magnetic NPs was measured to be 53.41 emu g^{-1}, suggesting a high magnetite content in the core-shell magnetic NPs. As can be seen clearly from the magnetic hysteresis loop (Fig. 5), the core-shell magnetic NPs exhibit superparamagnetism at room temperature, which depicts no magnetization remained when the applied magnetic field is removed. This is because of the small size magnetic NPs in the core.[27] Taking advantage of the strong magnetic properties, the core-shell NPs should be able to be easily separated from reaction solution if we apply an external magnetic field. As demonstrated in the photographs in Fig. 5, the core-shell magnetic NPs showed a tendency to be attracted toward the magnet and the suspended reaction solution turned transparent within seconds, revealing the excellent separability of the Au-Fe_3O_4@MIL-100(Fe) core-shell magnetic catalysts in the liquid-phase reactants and products. The superparamagnetism nature of the Au-Fe_3O_4@MIL-100(Fe) enable a fast and efficient separation of the catalysts from the mixture with the aid of an applied magnetic field.

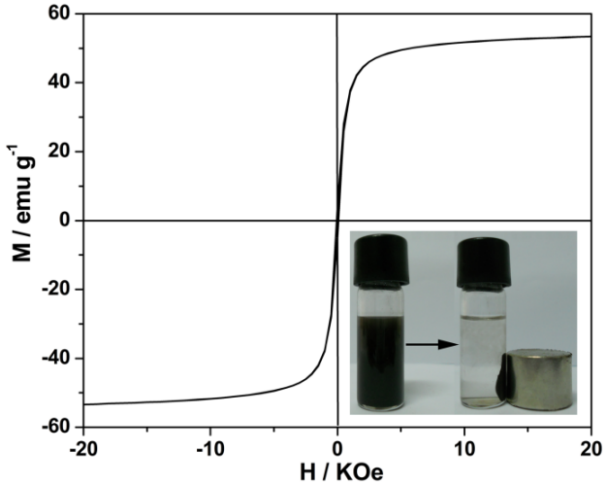

Fig. 5 The magnetic hysteresis loop of the as-synthesized Au-Fe_3O_4@MIL-100(Fe) core-shell magnetic NPs after 30 assembly cycles. The photographs in the inset demonstrate the convenient separation of the catalysts by an external magnetic field.

Liquid-phase reduction of 4-NP by $NaBH_4$ in the presence of noble metal NPs as catalysts has been intensively investigated for the efficient production of 4-AP.[8,33] We also chose this reaction as a model system to evaluate the catalytic activity of the Au-Fe_3O_4@MIL-100(Fe) core-shell magnetic NPs. Time-resolved UV-vis spectra of the reaction mixture solution was used to monitor the reduction kinetics. In the absence of catalysts, the reduction does not proceed even with a large excess of $NaBH_4$. After the catalysts of Au-Fe_3O_4@MIL-100(Fe) core-shell magnetic NPs were added into the reaction system, as shown in Fig. S3, the absorption intensity at 400 nm decreased quickly along with a concomitant absorption intensity at 300 nm increase with reaction time, indicating the reduction of 4-NP and formation of 4-AP, respectively. Since the concentration of $NaBH_4$ added in the system is much higher in comparison with that of 4-NP, the reduction can be considered as a pseudo-first-order reaction with regard to 4-NP only.[33] Fig. 6 shows the linear relationship of $\ln(C_t/C_0)$ as a function of reaction time t for the 4-NP reduction catalyzed by four core-shell Au-Fe_3O_4@MIL-100(Fe) magnetic catalysts with different shell thicknesses. The values of kinetic rate constant k can be calculated from the rate equation $\ln(C_0/C_t) = kt$, and all these plots match the pseudo-first-order reaction kinetics very well (Table 1). Impressively, among all these catalysts, the core-shell Au-Fe_3O_4@MIL-100(Fe) magnetic catalysts with 5 assembly cycles exhibit the highest activity with a rate constant estimated to be 5.53 min^{-1}, which is 2 and 168 times higher than that of Au-Fe_3O_4 and MIL-100(Fe), respectively, suggesting that the higher catalytic efficiencies for Au catalysts confined in MOF shells with ordered mesopores. Although the value of rate constant deceased significantly from 5.53 min^{-1} to 0.51 min^{-1} after 30 assembly cycles, the value is still superior to most Au-based catalysts.[34-36] The diffusion of reactants through the pores of MOF shell is believed to be

responsible for the decreased catalytic efficiency with the increasing number of assembly cycles. This comparison demonstrates that the shell thickness is a key factor in determining the test results. Although thicker shell is beneficial to stabilize the catalysts, over-thick shell must be avoided because diffusion constraint effects of porous shell may lead to significant decrease in catalytic activity.

Table 1 Comparison of kinetic constant (k) of 4-NP reduction by Au-Fe_3O_4, MIL-100(Fe), and core-shell Au-Fe_3O_4@MIL-100(Fe) magnetic catalysts with different assembly cycles.

Catalyst	k (min^{-1})
Au-Fe_3O_4	2.92
MIL-100(Fe)	0.032
Au-Fe_3O_4@MIL-100(Fe) (5 cycles)	5.53
Au-Fe_3O_4@MIL-100(Fe) (10 cycles)	1.71
Au-Fe_3O_4@MIL-100(Fe) (20 cycles)	0.81
Au-Fe_3O_4@MIL-100(Fe) (30 cycles)	0.51

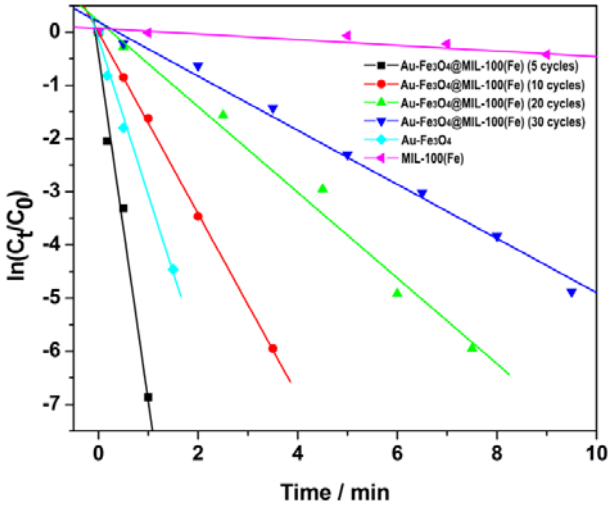

Fig. 6 Relationship of the ln(C_t/C_0) and reaction time t for the reduction of 4-NP to 4-AP over Au-Fe_3O_4, MIL-100(Fe), and core-shell Au-Fe_3O_4@MIL-100(Fe) magnetic catalysts after 5, 10, 20 and 30 assembly cycles, respectively.

Recyclability is one of the most important issues in the practical application of catalysts. As we all know that NP-based heterogeneous catalysts suffer from both low efficiency ofseparation and reduced catalytic activity resulting from NPs coagulation in liquid-phase reductions.[8] The core-shell structures described here are designed to overcome these challenges. With high saturation magnetization, our Au-Fe_3O_4@MIL-100(Fe) can be easily separated in a few seconds using an external magnetic field. After the catalyst was separated, washed with ethanol and dried at 75 °C, it can be used for another consecutive run without further treatment needed. Fig. 7 compares the catalytic performance of Au-Fe_3O_4 without and with the protection of a porous MOF shell in five successive cycles of reaction, respectively. In the first cycle, the Au-Fe_3O_4 unprotected catalysts show high activity due to the catalysis without experiencing much aggregation and the diffusion of reactants through porous MOF shell into the core is easy. However, the conversion ratio drops rapidly in the subsequent cycles of reaction. As can be seen from Fig. 7a and Fig. S5a, the conversion ratio drops to 4% only and the values of kinetic rate constant k decreases significantly from 2.92 to 0.02 min^{-1} after five consecutive reuses (Table S1†). In contrast, the Au catalysts protected by porous MOF maintain their activities well in the five successive catalytic cycles. The conversion ratio of 4-NP dropped only 20% for the sample of Au-Fe_3O_4@MIL-100(Fe) with 5 assembly cycles (Fig. 7b). The corresponding k value decreases from 5.53 to 1.57 min^{-1} (Table S2†). Interestingly, for the sample of Au-Fe_3O_4@MIL-100(Fe) with more assembly cycles, for instance, 30 assembly cycles, although the initial value of rate constant k (0.51 min^{-1}) is much lower than that of Au-Fe_3O_4@MIL-100(Fe) with 5 assembly cycles (5.53 min^{-1}), the conversion rate maintains with much better level. After five consecutive catalytic runs, the conversion rate only drops by 5% (Fig. S6†), and the k value changes from 0.51 to 0.26 min^{-1} (Table S3†). The results clearly demonstrate that the porous MOF shell protected catalysts are much more durable than the unprotected Au catalysts in the reaction cycles. Moreover, the TEM images of Au-Fe_3O_4@MIL-100(Fe) after five catalytic cycles show no obvious change in both size and morphology as compared to those of the catalyst before the reaction (Fig. S7, ESI†). The uniform distribution of Au NPs core with no distinct aggregation after catalytic reaction confirms the advantage of the confinement effect of the MOF shell. These findings indicate that the core-shell Au-Fe_3O_4@MIL-100(Fe) magnetic catalyst is stable under the current 4-NP reduction reaction condition and can be reused for multiple rounds of the reduction reaction. All these results suggest that our core-shell magnetic catalysts system has two advantages over the traditional metal nanocatalysts. First, the Au catalysts can be recovered easily from the reaction solution by using an external magnetic field, which can eliminate the necessity of filtration and centrifugation. Second, the porous MOF shell can effectively stabilize the Au NPs, making the catalysts reusable after multiple cycles of reaction.

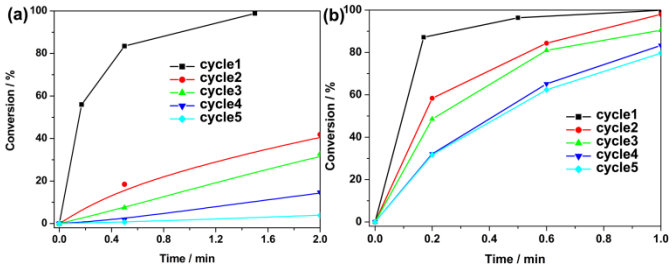

Fig. 7 Activity reproducibility tests for 5 cycles of 4-NP reduction under the same reaction conditions over the Au-Fe_3O_4 magnetic NPs (a), and the core-shell Au-Fe_3O_4@MIL-100(Fe) magnetic NPs synthesized with five assembly cycles (b).

On the basis of above experimental results and the relevant literature, the catalytic reduction process can be elucidated as follows: according to traditional theory about the reduction of 4-NP, electron transfer takes place from BH_4^- to 4-NP through adsorption of the reactant molecules onto the Au catalysts surface, the catalytic efficiency is highly dependent on the large surface areas of Au NPs.[37] In this work, the 4-NP can be adsorbed onto the mesoporous MIL-100(Fe) via π-π stacking

interactions because 4-NP is π-rich in nature.[38] Such adsorption provides a high concentration of 4-NP near to the interface of the Au NPs and MIL-100(Fe), leading to highly efficient contact between them. The electron transfers from borohydride/borate to the catalysts and subsequently transfers to the adsorbed 4-NP. Then the hydrogen atom transfers from BH_4^-/solvent to the 4-NP, resulting in the formation of 4-AP. Finally, the products of 4-AP are desorbed from the surface of the catalysts to the solution through the channels of the MOF shell.[39]

The catalytic activity of metal NPs is usually affected by various factors, especially the interactions between metal NPs and their supports.[33] Core-shell structures of NPs normally exhibit superior activity in heterogeneous catalysis due to the interaction between the core and shell, which can further modify the electronic structure of the NPs.[40-42] The present work demonstrate that the catalytic activity of the core-shell Au-Fe_3O_4@MIL-100(Fe) magnetic catalysts with 5 assembly cycles is much higher than those of bare Au-Fe_3O_4 and pure MIL-100(Fe). This prominent catalytic activity might also be attributed to the modification of the electronic structure of Au NPs in the core-shell structures. To shed light on the remarkable reduction of 4-NP over Au-Fe_3O_4@MIL-100(Fe), the catalysts including Au-Fe_3O_4, MAA-Au-Fe_3O_4 and Au-Fe_3O_4@MIL-100(Fe) were investigated by XAS. Both X-ray absorption near-edge structure (XANES) and extended X-ray absorption fine structure (EXAFS) spectra were collected at the Au L_3-edge. Fig. S8 shows the normalized Au L_3-edge XANES spectra for the Au-Fe_3O_4, MAA-Au-Fe_3O_4 and core-shell Au-Fe_3O_4@MIL-100(Fe) magnetic NPs. The intensity of the white line, which is the first peak at the Au L_3-edge XANES spectra is known to arise from electron transitions to unoccupied 5d states.[43] Therefore, any variations of the density of unoccupied states due to changes in the oxidation state will be reflected in the intensity of the white line. Compared with pure Au-Fe_3O_4, MAA-functionalized Au-Fe_3O_4 NPs show enhanced white line absorption. However, when the MAA-Au-Fe_3O_4 NPs coated with MIL-100(Fe) shell, the intensity of the white line drops. (Fig. S8, insert). This observation reveals that the electronic properties of surface Au atoms in the Au-S interfaces are truly modified after being coated with the MOF shell due to the electron transfer from MIL-100(Fe) to Au.[44] The results of Fourier transformation (FT) of the EXAFS signals are summarized in Fig. 8 and Table S4. Similar to the recently reported,[45] the oscillation $k^2\chi(k)$ functions for the three Au NPs show a remarkable difference in the low k region (k = 4-6 Å), which can be ascribed to the distinct interactions between Au and S atoms (Fig. 8a). Furthermore, the difference can be seen clearly in Fig 8b, the intensity of Au-S peak gradually increases in the order of MAA-Au-Fe_3O_4 > Au-Fe_3O_4@MIL-100(Fe) > Au-Fe_3O_4, along with a blue shift of the position. Moreover, from Table S4, we can easily find that the coordination numbers of Au-Au bond display an obviously reduction with the order of Au-Fe_3O_4 > Au-Fe_3O_4@MIL-100(Fe) > MAA-Au-Fe_3O_4. It is due to the electron transfer from MIL-100(Fe) to Au. From the XAFS results we can find that the electron donation from MIL-100(Fe) to Au NPs will make MIL-100(Fe) more acidic (Lewis acid), which facilitates the activation of H_2 (Lewis base) molecules through Lewis acid to base interaction, thus leading to the improved catalytic activity of the core-shell catalyst, similar to those reported in the literature.[46] Therefore the Au-Fe_3O_4@MIL-100(Fe) catalysts present a prominent catalytic activity for the reduction of 4-NP at room temperature. Then, it can be concluded that the remarkable catalytic activity of Au-Fe_3O_4@MIL-100(Fe) is mainly due to a synergistic effect between Au and MIL-100(Fe).

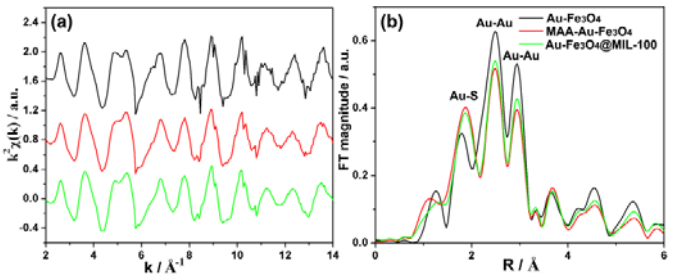

Fig. 8 Au L_3-edge k^2-weighted extended X-ray absorption fine structure oscillations [$k^2\chi(k)$] (a) and their Fourier transforms (b) for Au-Fe_3O_4, MAA-Au-Fe_3O_4, and Au-Fe_3O_4@MIL-100(Fe) core-shell magnetic NPs.

Conclusions

In summary, this study demonstrates an effective strategy for the fabrication of novel core-shell Au-Fe_3O_4@MIL-100(Fe) magnetic catalysts through a versatile layer-by-layer assembly method and the MOF shell thickness can be controlled by altering the number of assemble cycles. These core-shell magnetic catalysts are found to exhibit excellent catalytic performance toward 4-NP reduction. Compared to other Au-based heterogeneous catalysts, these core-shell magnetic structure catalysts are ideal recyclable catalysts for liquid-phase reactions due to their superparamagnetic components for efficient magnetic separation and a porous MOF shell for stabilization of the encapsulated Au NPs. Such core-shell catalysts are expected to be used in industrial applications, where separation and recycling are critically required to reduce the cost as well as waste production. More importantly, with the merits of easy separation and flexible control over size, structure and composition of the metallic nanosatellites, this simple and versatile method might provide a multitude of magnetic catalysts for broad applications in more interesting reactions in the future.

Acknowledgements

This work is supported by the National Basic Research Program of China (2013CB834605, 2010CB923302) and the National Natural Science Foundation of China (Grant Nos. U1232102, 21473178).

Notes and references

[a] National Synchrotron Radiation Laboratory and Collaborative Innovation Center of Suzhou Nano Science and Technology, University of Science and Technology of China, Hefei 230029 (P.R. China). Fax: (+86)-551-5141078; E-mail: jfzhu@ustc.edu.cn

[b] Department of Applied Chemistry, Anhui Agricultural University, Hefei 230036 (P.R. China).

† Electronic Supplementary Information (ESI) available: [details of any supplementary information available should be included here]. See DOI: 10.1039/b000000x/

References

[1] K. C. F. Leung, S. H. Xuan, X. M. Zhu, D. W. Wang, C. P. Chak, S. F. Lee, W. K. W. Ho and B. C. T. Chung, *Chem. Soc. Rev.,* 2012, **41**, 1911-1928.

[2] J. Liu, S. Z. Qiao, Q. H. Hu and G. Q. Lu, *Small,* 2011, **7,** 425-443.

[3] S. Shylesh, V. Schunemann and W. R. Thiel, *Angew. Chem. Int. Ed.,* 2010, **49,** 3428-3459.

[4] N. A. Frey, S. Peng, K. Cheng and S. H. Sun, *Chem. Soc. Rev.,* 2009, **38,** 2532-2542.

[5] S. Shylesh, J. Schweizer, S. Demeshko, V. Schunemann, S. Ernst and W. R. Thiel, *Adv. Synth. Catal.,* 2009, **351,** 1789-1795.

[6] Y. M. Zhai, L. Han, P. Wang, G. P. Li, W. Ren, L. Liu, E. K. Wang and S. J. Dong, *ACS Nano,* 2011, **5,** 8562-8570.

[7] Z. C. Xu, Y. L. Hou and S. H. Sun, *J. Am. Chem. Soc.,* 2007, **129,** 8698-8699.

[8] J. P. Ge, Q. Zhang, T. R. Zhang and Y. D. Yin, *Angew. Chem. Int. Ed.,* 2008, **47,** 8924-8928.

[9] K. M. Yeo, J. Shin and I. S. Lee, *Chem. Commun.,* 2010, **46**, 64-66.

[10] J. Lee, J. Yang, H. Ko, S. J. Oh, J. Kang, J. H. Son, K. Lee, S. W. Lee, H. G. Yoon, J. S. Suh, Y. M. Huh and S. Haam, *Adv. Funct. Mater.,* 2008, **18,** 258-264.

[11] H. C. Zhou, J. R. Long and O. M. Yaghi, *Chem. Rev.,* 2012, **112,** 673-674.

[12] J. R. Li, J. Sculley and H. C. Zhou, *Chem. Rev.,* 2012, **112,** 869-932.

[13] Y. J. Cui, Y. F. Yue, G. D. Qian and B. L. Chen, *Chem. Rev.,* 2012, **112,** 1126-1162.

[14] P. Horcajada, T. Chalati, C. Serre, B. Gillet, C. Sebrie, T. Baati, J. F. Eubank, D. Heurtaux, P. Clayette, C. Kreuz, J. S. Chang, Y. K. Hwang, V. Marsaud, P. N. Bories, L. Cynober, S. Gil, G. Ferey, P. Couvreur and R. Gref, *Nat. Mater.,* 2010, **9,** 172-178.

[15] K. M. L. Taylor-Pashow, J. Della Rocca, Z. G. Xie, S. Tran and W. B. Lin, *J. Am. Chem. Soc.,* 2009, **131,** 14261-14263.

[16] P. Horcajada, C. Serre, G. Maurin, N. A. Ramsahye, F. Balas, M. Vallet-Regi, M. Sebban, F. Taulelle and G. Ferey, *J. Am. Chem. Soc.,* 2008, **130,** 6774-6780.

[17] P. Horcajada, C. Serre, M. Vallet-Regi, M. Sebban, F. Taulelle and G. Ferey, *Angew. Chem. Int. Ed.,* 2006, **45,** 5974-5978.

[18] A. Dhakshinamoorthy, M. Alvaro and H. Garcia, *Chem. Commun.,* 2012, **48,** 11275-11288.

[19] A. Corma, H. Garcia and F. Xamena, *Chem. Rev.,* 2010, **110,** 4606-4655.

[20] Y. Y. Pan, B. Z. Yuan, Y. W. Li and D. H. He, *Chem. Commun.,* 2010, **46,** 2280-2282.

[21] T. Ishida, M. Nagaoka, T. Akita and M. Haruta, *Chem. Eur. J.,* 2008, **14,** 8456-8460.

[22] Y. K. Hwang, D. Y. Hong, J. S. Chang, S. H. Jhung, Y. K. Seo, J. Kim, A. Vimont, M. Daturi, C. Serre and G. Ferey, *Angew. Chem. Int. Ed.,* 2008, **47,** 4144-4148.

[23] J. Hermannsdorfer, M. Friedrich, N. Miyajima, R. Q. Albuquerque, S. Kummel and R. Kempe, *Angew. Chem. Int. Ed.,* 2012, **51,** 11473-11477.

[24] C.-H. Kuo, Y. Tang, L.-Y. Chou, B. T. Sneed, C. N. Brodsky, Z. Zhao and C.-K. Tsung, *J. Am. Chem. Soc.,* 2012, **134,** 14345-14348.

[25] G. Lu, S. Z. Li, Z. Guo, O. K. Farha, B. G. Hauser, X. Y. Qi, Y. Wang, X. Wang, S. Y. Han, X. G. Liu, J. S. DuChene, H. Zhang, Q. C. Zhang, X. D. Chen, J. Ma, S. C. J. Loo, W. D. Wei, Y. H. Yang, J. T. Hupp and F. W. Huo, *Nat. Chem.,* 2012, **4,** 310-316.

[26] F. Ke, J. Zhu, L.-G. Qiu and X. Jiang, *Chem. Commun.,* 2013, **49,** 1267-1269.

[27] Y. H. Deng, C. H. Deng, D. W. Qi, C. Liu, J. Liu, X. M. Zhang and D. Y. Zhao, *Adv. Mater.,* 2009, **21,** 1377-1382.

[28] Z. M. Cui, L. Y. Hang, W. G. Song and Y. G. Guo, *Chem. Mater.,* 2009, **21,** 1162-1166.

[29] P. Horcajada, S. Surble, C. Serre, D. Y. Hong, Y. K. Seo, J. S. Chang, J. M. Greneche, I. Margiolaki and G. Ferey, *Chem. Commun.,* 2007, 2820-2822.

[30] L. He, Y. Liu, J. Liu, Y. Xiong, J. Zheng, Y. Liu and Z. Tang, *Angew. Chem. Int. Ed.,* 2013, **52,** 3741-3745.

[31] S. J. Gregg and K. S. W. Sing, *Adsorption, Surface Area and Porosity,* Academic Press, London, 1997, 111-194.

[32] R. Canioni, C. Roch-Marchal, F. Secheresse, P. Horcajada, C. Serre, M. Hardi-Dan, G. Ferey, J. M. Greneche, F. Lefebvre, J. S. Chang, Y. K. Hwang, O. Lebedev, S. Turner and G. Van Tendeloo, *J. Mater. Chem.,* 2011, **21,** 1226-1233.

[33] H. L. Jiang, T. Akita, T. Ishida, M. Haruta and Q. Xu, *J. Am. Chem. Soc.,* 2011, **133,** 1304-1306.

[34] X. Guo, Q. Zhang, Y. H. Sun, Q. Zhao and J. Yang, *ACS Nano,* 2012, **6,** 1165-1175.

[35] F. Dong, W. Guo, S. K. Park and C. S. Ha, *Chem. Commun.,* 2012, **48,** 1108-1110.

[36] Y. W. Zhang, S. Liu, W. B. Lu, L. Wang, J. Q. Tian and X. P. Sun, *Catal. Sci. Technol.,* 2011, **1,** 1142-1144.

[37] P. Zhang, C. L. Shao, Z. Y. Zhang, M. Y. Zhang, J. B. Mu, Z. C. Guo and Y. C. Liu, *Nanoscale,* 2011, **3,** 3357-3363.

[38] W. B. Lu, R. Ning, X. Y. Qin, Y. W. Zhang, G. H. Chang, S. Liu, Y. L. Luo and X. P. Sun, *J. Hazard. Mater.,* 2011, **197,** 320-326.

[39] S. Gazi and R. Ananthakrishnan, *Appl. Catal. B-Environ.,* 2011, **105,** 317-325.

[40] V. Mazumder, M. Chi, K. L. More and S. H. Sun, *J. Am. Chem. Soc.,* 2010, **132,** 7848-7849.

[41] S. Alayoglu, A. U. Nilekar, M. Mavrikakis and B. Eichhorn, *Nat. Mater.,* 2008, **7,** 333-338.

[42] J. R. Kitchin, J. K. Norskov, M. A. Barteau and J. G. Chen, *Phys. Rev. Lett.,* 2004, **93,** 156801-156804.

[43] Y. Mikhlin, M. Likhatski, Y. Tomashevich, A. Romanchenko, S. Erenburg and S. Trubina, *J. Electron Spectrosc. Rel. Phenom.,* 2010, **177,** 24-29.

[44] J. He, Z. Yan, J. Wang, J. Xie, L. Jiang, Y. Shi, F. Yuan, F. Yu and Y. Sun, *Chem. Commun.,* 2013, **49,** 6761-6763.

[45] Y. Jiang, P. Yin, Y. Li, Z. Sun, Q. Liu, T. Yao, H. Cheng, F. Hu, Z. Xie, B. He, G. Pan and S. Wei, *J. Phys. Chem. C,* 2012, **116,** 24999-25003.

[46] J. M. Song, S. S. Zhang and S. H. Yu, *Small,* 2013, **10,** 717-724.